Available online at www.sciencedirect.com
ScienceDirect
Journal of Organometallic Chemistry 693 (2008) 1203–1214
Journal of Organometallic Chemistry
www.elsevier.com/locate/jorganchem

An experimental and a DFT study on the synthesis, spectroscopic characterization, and reactivity of the adducts of dimethyl- and diphenyltin(IV) dichlorides with γ-pyrones [4*H*-pyran-4-one (PYR) and 2,6-dimethyl-4*H*-pyran-4-one (DMP)]: Crystal structure of Ph_2SnCl_2(PYR)

Hariklia Papadaki [a], Aristides Christofides [a,*], Evangelos G. Bakalbassis [b,*], John C. Jeffery [c]

[a] *Department of Chemistry, Section of General and Inorganic Chemistry, Aristotle University of Thessaloniki, P.O. Box 135, 54 124 Thessaloniki, Greece*
[b] *Department of Chemistry, Laboratory of Applied Quantum Chemistry, Aristotle University of Thessaloniki, P.O. Box 135, 54 124 Thessaloniki, Greece*
[c] *School of Chemistry, Section of Inorganic Chemistry, The University of Bristol, Bristol BS8 ITS, England, United Kingdom*

Received 7 November 2007; received in revised form 9 January 2008; accepted 9 January 2008
Available online 16 January 2008

Abstract

The Sn(IV) R_2SnCl_2(γ-pyrone)$_n$ [R = Me or Ph; γ-pyrone = 4*H*-pyran-4-one (PYR) or 2,6-dimethyl-4*H*-pyran-4-one (DMP); $n = 1$ or 2] adducts have been synthesized and investigated. The adducts Ph_2SnCl_2(PYR) (**1**), $Me_2SnCl_2(PYR)_2$ (**2**), Ph_2SnCl_2(DMP) (**3**) and Me_2SnCl_2(PYR)(PNO) (**4**), (PNO = 4-methylpyridine *N*-oxide) have been prepared by the addition of the corresponding γ-pyrone to chloroform solution of R_2SnCl_2. The new compounds have been characterized by elemental analysis and spectroscopic (IR, ^{1}H, ^{13}C NMR and Mössbauer) means. The single-crystal diffraction study of **1** shows the Sn(IV) to be five-coordinate, [Sn–O and Sn–Cl(1), Sn–Cl(2) distances of 2.3190(13) and 2.4312(6), 2.3653(7), respectively], and the Cl–Sn–Cl bond angle to be 91.17°. The reactivity of **2** towards bipy, Ph_3PO, QNO (Q = quinoline) resulted in complete displacement of PYR and formation of already known compounds whereas, the PNO displaced only one equivalent of PYR, causing the preparation of the new mixed complex **4**, possibly through a S_N1 formation mechanism. DFT/B3LYP molecular orbital calculations were carried out for the **1**–**4** complexes, their precursors, Ph_2SnCl_2, (**5**) and Me_2SnCl_2, (**6**) and the ligands, PYR, DMP and PNO in an attempt to explain the structures and reactivity of the complexes. Optimized resulting geometries, vibrational frequencies, and the electron-accepting ability of the complexes and the precursors towards nucleophiles are discussed.

Keywords: Adducts of tin(IV); Carbonyl ligands; 4*H*-Pyran-4-one; 2,6-Dimethyl-4*H*-pyran-4-one; Density functional calculations

1. Introduction

The complexes of 2,6-dimethyl-4*H*-pyran-4-one (DMP) with various metal salts have long been known [1]. Later on the lanthanide complexes of the same γ-pyrone, generally having octahedral symmetry, have been isolated [2]. Mercury(II) compounds of the formulae $[Hg(DMP)X_2]_n$ and $(HgX_2)_3(DMP)_2$ (X = Cl or Br) have been prepared [3], the incorporated DMP being weakly bound to the metal. Twelve years ago tin adducts of the types $Sn(DMP)_2Cl_2$ and $Sn(DMP)_2Cl_4$ were prepared by Fregona et al. [4]. So far we have been reviewing the coordination chemistry of DMP, and one might think that there have been no reports on organometallic compounds of the ligand in question. However, the survey of the literature reveals only one paper [5], dealing with the synthesis of the organotin complexes $PhSn(DMP)Cl_3$, $Ph_2Sn(DMP)Cl_2$,

* Corresponding authors. Tel.: +30 2310 997695; fax: +30 2310 997837.
E-mail address: bakalbas@chem.auth.gr (E.G. Bakalbassis).

0022-328X/$ - see front matter © 2008 Elsevier B.V. All rights reserved.
doi:10.1016/j.jorganchem.2008.01.014

$Ph_3Sn(DMP)Cl$, $Me_2Sn(DMP)X_2$ (X = Cl or Br) and $Me_2Sn(DMP)_2Cl_2$. Although no X-ray data is appeared in that paper, it is reported that in all the above compounds the DMP ligand is coordinated to the metal via the carbonyl oxygen, causing a low energy shift of ν(C=O) as expected.

Continuing our work on organotin adducts with oxygen donor ligands [6], herein we report on the synthesis and the spectroscopic characterization of four complexes. Three of them incorporate 4*H*-pyran-4-one (PYR), for which, as far as we know there have been no reports on tin organometallic complexes, whereas the other one includes DMP. The X-ray, single-crystal diffraction study of the adduct $Ph_2SnCl_2(PYR)$ is also reported, along with the reactivity of $Me_2SnCl_2(PYR)_2$ towards some ligands. To the best of our knowledge, this is the first X-ray structure ever reported on the Sn(IV) organometallic complexes incorporating the pyrone ligand (4*H*-pyran-4-one), which, from the two known coordination modes – (i) via the carbonyl oxygen [7,8], or (ii) through both the carbonyl oxygen and the ortho carbon atom of its ring [9] – prefers the first one. Lack of X-ray structural data for most of the complexes under examination, led to theoretical B3LYP/LANL2DZ studies on the structure and reactivity of all complexes under study, their precursors and their ligands.

It is worth mentioning here that, the anticancer profile of many diorganotin compounds, R_2SnX_2, in combination with the nature of the R groups and of the X ligands has been investigated [10]. In relation with the above, we hope that our reactions may help in understanding how tin(IV) tetracoordinate species may bind to DNA by acquiring penta- or hexacoordinate structures [11]. On the other hand, it is known that some dialkyl organotin compounds exhibit catalytic activity in the production of polyurethane foam and in the vulcanization of silicones [12]. This is another field in which our compounds might find some application.

2. Results and discussion

2.1. Synthesis

Treatment of a chloroform solution of Me_2SnCl_2 with PYR in 1:2 molar ratio, affords the adduct **2** (Eq. (1)). The reaction of a chloroform solution of adduct **2** with 4-methylpyridine *N*-oxide (PNO) in 1:1 molar ratio results in displacement of one equivalent of PYR and the formation of the mixed complex **4** (Eq. (2)). The adducts **1** and **3** are formed by the reaction of the Lewis acid Ph_2SnCl_2 with PYR and DMP, respectively, in 1:1 molar ratio in the above solvent (Eq. (3)).

$$Me_2SnCl_2 + 2PYR \rightarrow Me_2SnCl_2(PYR)_2\ (\mathbf{2}) \quad (1)$$

$$Me_2SnCl_2(PYR)_2 + PNO \rightarrow Me_2SnCl_2(PYR)(PNO)\ (\mathbf{4}) + PYR \quad (2)$$

$$Ph_2SnCl_2 + L \rightarrow Ph_2SnCl_2L\ [\mathbf{1}\ (L = PYR)\ \text{or}\ \mathbf{3}\ (L = DMP)] \quad (3)$$

It should be stressed out here that, despite our numerous attempts, we failed to grow single-crystals proper for a X-ray structural study for all but one (**1**) complexes.

2.2. X-ray structural analysis of $Ph_2SnCl_2(PYR)$ (*1*)

The molecular structure of the adduct **1**, is shown in Fig. 1 together with the atomic numbering scheme. Selected bond lengths and angles are listed in Table 1.

An examination of the packing diagram reveals no unusual intermolecular contacts. Thus, there is a discrete pentacoordinated molecule of trigonal-bipyramidal geometry in which the two C atoms of two phenyl groups and one chlorine atom are located at equatorial positions; the other Cl atom and the carbonyl O atom of the PYR ligand occupy the axial positions. The two phenyl rings are mutually twisted with respect to the equatorial plane [defined by Cl(2), C(11) and C(21)] probably to avoid steric congestion.

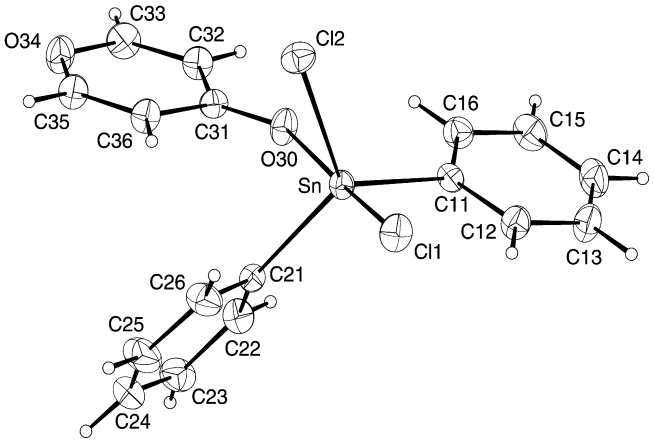

Fig. 1. Molecular structure of **1** with the atom-labeling scheme.

Table 1
Selected bond lengths (Å) and angles (°) for **1**

Sn–C(21)	2.121 (2)
Sn–C(11)	2.133 (2)
Sn–O(30)	2.3190 (13)
Sn–Cl(2)	2.3653 (7)
Sn–Cl(1)	2.4312 (6)
C(11)–C(12)	1.395 (3)
C(11)–C(16)	1.400 (3)
C(21)–C(22)	1.387 (3)
C(21)–Sn–C(11)	127.29 (7)
C(21)–Sn–O(30)	85.59 (6)
C(11)–Sn–O(30)	85.59 (6)
C(21)–Sn–Cl (2)	114.25 (5)
C(11)–Sn–Cl (2)	115.84 (5)
O(30)–Sn–Cl (2)	82.46 (4)
C(21)–Sn–Cl (1)	96.19 (5)
C(11)–Sn–Cl (1)	98.15 (5)
O(30)–Sn–Cl (1)	173.56 (4)
Cl(2)–Sn–Cl(1)	91.17 (2)
C(31)–O(30)–Sn	133.63 (12)
O(30)–C(31)–C(32)	120.2 (2)
O(30)–C(31)–C(36)	125.1(2)
C(32)–C(31)–C(36)	114.7 (2)

The dihedral angles between the rings defined by C(11), C(16) and C(21), C(26) and the trigonal plane are 106° and 43°, respectively. The pyrone ring is not positioned between the two phenyl groups when viewed along the apical O–Sn–Cl axis, thereby avoiding steric encumbrance, whereas in Ph_2SnCl_2 (2,6-$Me_2C_5H_3NO$) [13], the pyridine ring for the same reasons lies directly below the Cl atom of the trigonal plane. The Sn atom does not lie exactly in the equatorial trigonal plane, but is displaced towards the Cl atom by ca 0.15 Å. The Cl–Sn–O angle is 173.56(4)°, and the sum of the equatorial angles in the trigonal girdle subtended at tin by the two ipso carbons and the Cl(2) is 357.38°. The Sn–O–C angle is 133.63(12)° and is larger than the corresponding Sn–O–N in Ph_2SnCl_2 (2,6-$Me_2C_5H_3NO$) [13] [125.7(2)°]. The tin oxygen distance here is 2.3190(13) Å and is longer than the corresponding lengths of Me_2-Sn-$Cl_2(QNO)_2$ [2.220(2) Å] [14], $Me_2SnCl_2(PyNO)_2$ [2.251(16) Å] [15] and Me_2SnCl_2(4-PhPyNO)$_2$ [2.227(2) Å] [6], indicating perhaps better coordination for aromatic *N*-oxides. The same distance is shorter than the corresponding lengths in the hexacoordinated adducts of dimethyl tin(IV) dichloride with cyclopropenone [2.380(2)] [16] and salicylaldehyde 2.680(12)] [17].

2.3. Reactivity

The behaviour of $Me_2SnCl_2(PYR)_2$, **2** towards some ligands has been examined (Scheme 1).

The reactions of adduct **2** with bipy or QNO and Ph_3PO in 1:1 and 1:2 molar ratios, respectively, result in displacement of PYR and formation of the corresponding previously reported compounds [14,18]. As expected, the same product was received by the reaction of QNO with adduct **2** in 2:1 molar ratio. Addition of 1 mol of 4-methylpyridine *N*-oxide (PNO) to complex **2** leads to novel mixed complex **4**, whilst reactions with 4-dimethylaminopyridine (4-Me_2NPy) and 4-cyanopyridine *N*-oxide (4-CNPyNO) do not give clear cut results. This seems to indicate that the coordination capacity of PYR towards Sn(IV) is almost equal to that of PNO and lower than those of the ligands which displace it completely.

2.4. IR spectra

The infrared spectrum of the employed free PYR ligand appears strong absorptions at 1658 and 1640 asymmetric, 1609 cm^{-1} symmetric assignable to ν(C=O) and ν(C=C), respectively [19,20], whereas the free DMP shows the corresponding frequencies [19] at 1609 and 1670 cm^{-1}. In the complexes of PYR the ν(C=O) occurs at the 1580–1560 cm^{-1} range and is shifted to lower energy by ca 92 cm^{-1}, as compared to that of the free ligand. The ν(C=C) of the same complexes occurs at ca. 1638 cm^{-1}, probably the asymmetric one, and seems to be insensitive to complexation. The DMP adduct (**3**) shows two strong absorptions at 1651 and 1539 cm^{-1}, assignable to ν(C=C) and ν(C=O), respectively, the former being shifted to lower energy by 18 cm^{-1}, whereas the latter by 70 cm^{-1}. The IR data for the adduct **3** is almost identical with that for the same compound [5]. These main absorptions of the used ligands appear a change in ordering upon complexation, as it has been observed by others [21] in the case of Al and Ga complexes with several 3-hydroxyl-4-pyrones.

The single Sn–Me stretching frequencies at 582 and 567 cm^{-1} for six coordinate adducts **2** and **4**, respectively, are indicative of *trans*-methyl configuration [18]. However, we cannot be sure for the chlorine atoms of the same adducts (pointing to a *trans* configuration), because the apparently single bands around 266 cm^{-1} are not well resolved. The **1** and **3** adducts appear absorptions at ca. 337 and 270 cm^{-1} assignable to ν(Sn–Cl), which indicate different orientations for the two chlorine atoms. In fact, the X-ray structure determination of **1** showed one Cl at the equatorial position, whereas the other occupies an axial one in a trigonal-bipyramidal environment. Moreover, the above bands appear in the same range with those occurring in other adducts bearing monodentate O-donors and having similar structure [5]. The infrared spectrum of **4** shows a strong intensity band at 390 cm^{-1}, probably belonging to ν(Sn–O).

2.5. NMR spectra

The ^{1}H NMR spectra af PYR adducts show doublets at ca 6.41 and 7.79 ppm, assignable to H_a and H_b hydrogens of the pyrone ring, respectively, being almost insensitive to complexation, only for **2** both signals are observed slightly down field with respect to those of the free ligand. The $^3J(^1H_a–^1H_b)$ values of **2** and **4**, and **1** are slightly increased and decreased, respectively, as compared to that of the free PYR, the larger decrease (0.92 Hz) was observed for adduct **1**. In the ^{1}H NMR spectrum of **3** the single peak

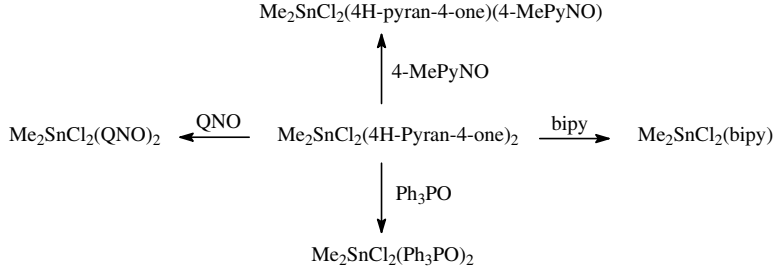

Scheme 1.

assignable to H_a of the DMP, do not exhibit any appreciable difference in chemical shift from that of the free DMP. The reason for these slight shifts for all the studied adducts may be, the partial dissociation of the ligands (PYR or DMP) in chloroform solutions. The above explanation was provided by others for analogous dimethyltin adducts, displaying the same behaviour [5]. The methyl hydrogens resonances (ca. 1.19 ppm) for **2** and **4** are close to those observed for the parent Lewis acid (1.22 ppm) in $CDCl_3$ solution. The ^2J (^{119}Sn–^1H) and ^2J (^{117}Sn–^1H) values are ca 83.3 and 79.8 Hz, respectively, being similar to those observed for hexacoordinate adducts of Me_2SnCl_2 with monodentate aromatic *N*-oxides [6]. Moreover, adduct **4** exhibits all the resonances due to 4-MePyNO.

In the ^{13}C NMR spectra of the investigated adducts the peaks due to all carbons of the pyrone rings can be seen, the majority of them show smaller slight shifts relative to those of the free ligands (PYR or DMP). In particular, the C(2) carbons of adducts **2** and **3** are shifted downfield by 0.9 and 1.8 ppm, respectively. The carbonyl carbons of the same adducts show more or less similar also behaviour, the effect being larger for **3** (δ ppm, 1.0). The cause for the above small or slight shift can be again the ligand dissociation, as in the case of the ^1H NMR spectra. The methyl carbons of dimethyl tin adducts (**2**, **4**) resonate at ca 10.9 ppm and are shifted downfield as compared to the analogous peak of Me_2SnCl_2 (6.6 ppm) in the same solvent ($CDCl_3$). The reason for this expected shift, which is not observed for the methyl hydrogen in the respective ^1H NMR spectra, has been explained elsewhere [6,22]. The ^2J (^{119}Sn–^1H) and ^1J (^{119}Sn–^{13}C) values of the adducts **2** and **4** are ca. 83.4 and 644.8 Hz, respectively, being remarkably increased relative to those of Me_2SnCl_2 (68.7 and 478 Hz) [6] in chloroform solutions. However, the same values are not as high as they could be expected for hexacoordinate adducts of the same Lewis acid with monodentate O-donors. For comparison, the ^2J (^{119}Sn–^1H) values for $Me_2SnCl_2$2L (L = PyNO, 4-ClPyNO, PNO) are ca 92.8 Hz in $CDCl_3$ [23], whereas the magnitude of ^1J(^{119}Sn–^{13}C), attributed to the formation of $Me_2SnCl_2 \cdot 2DMSO$ in DMSO solution of Me_2SnCl_2, is 1014.4 Hz [24]. Moreover, the coupling constants in question of adducts **2** and **4** are even lower than those of the analogous octahedral dimethyl tin compounds with monodentate *N*-oxides, reported in our earlier work [6] and for which significant complex dissociation in solution was confirmed by other data. The above situation indicates that the adducts **2** and **4** are largely dissociated in solution.

The examination of the ^{13}C NMR spectra of the substituted phenyl tin(IV) adducts **1** and **3** shows that the ipso carbon atoms of the phenyl rings exhibit small downfield shifts, relative to the corresponding of the free Lewis acid (136.8 ppm) [24], upon increase in coordination number of the tin atom from four to five, in $CDCl_3$ solutions. The ^1J(^{119}Sn–^{13}C) values are ca 908.2 Hz, being increased as compared to that of the Ph_2SnCl_2 (786 Hz). The above coupling constant of **3** is larger than that of **1** by 34.1 Hz; we think that the difference is too small to suggest that between the two employed pyrones, the DMP possesses better coordination ability, since the IR spectra have indicated the opposite.

2.6. ^{119}Sn Mössbauer data

The ^{119}Sn Mössbauer data for complexes **1**–**4** are listed in Table 2. The ρ values (ρ = QS/IS) obtained for all complexes indicate higher than four coordination number [25].

Inspection of the quadrupole splitting (QS) of the hexacoordinated complexes **2** and **4** show essential *trans*-[$SnMe_2$] arrangement for **4**, whereas for **2** its Mössbauer spectrum displaying two doubles indicated a mixture of 56% *trans*- and 44% *cis*-isomer. The parameters of the spectrum are consistent with *trans*- (*IS* 1.42, *QS* 4.20 mm s^{-1}) and *cis*- (IS 1.54, QS 3.63 mm s^{-1}), the assignment being made on the base that the *trans*- isomer possesses the larger QS value [26]. The existence of the *cis*-isomer in the solid state for complex **2** is further substantiated by the shape of the Sn–Cl stretching band at 270 cm^{-1} in the far-infrared region [27]. However, it must be pointed out that both compounds were assigned a *trans*-stereochemistry on the evidence of just one methyl resonance in their ^1H NMR spectra as measured in solution [25,26]. That brings about for **2** the unlike possibility of a *trans*- to *cis*-process, taken place to a certain degree on crystallization. In addition, its ^1H NMR spectrum do not support a fluxional behaviour which would make chemically equivalent the methyl groups. Based on the above arguments we cannot provide a clear answer for the behaviour of adduct **2**. The diphenyltin(IV) adducts **1** and **3** having trigonal-bipyramidal geometry, as showed the X-ray structure determination of **1**, appear a substantial difference in their quadrupole splitting values, the one of **1** being larger than that of **3**. This difference may be interpreted in terms of better coordination ability of PYR towards Sn(IV) than that of DMP [28], supported by the observation that between the two pentacoordinated adducts (**1**, **3**) the larger negative shift of ν(C–O) is obtained for **1**.

2.7. Evaluation of the proper computational level

It was shown above that there is only one X-ray crystal structure study for the one out of four complexes studied. In order to verify the actual relationships between the spectroscopic and structural features, as well as the electronic

Table 2
^{119}Sn Mössbauer Data for **1**–**4**

Compound	IS[a] (mm s^{-1})	QS[a] (mm s^{-1})	$\Gamma/2$[a] (mm s^{-1})		ρ (QS/IS)	T (K)
1	1.36	3.81	0.79		2.80	80
2	1.42	4.20	0.41	56%	2.96	80
	1.54	3.63		44%	2.36	
3	1.20	2.71	0.41		2.26	80
4	1.34	3.96	0.37		2.96	85

[a] Error ± 0.02 mm s^{-1}.

structure and reactivity of the complexes, an investigation was undertaken at the density functional theory (DFT) [29] level on all complexes, precursors and ligands involved in the present study. With the aim of evaluating a proper computational set-up, owing to the lack of structural experimental studies in the gas-phase for the same compounds, calculations have been carried out with different functionals and basis sets (BS's), on the only experimental structural data available, being the solid-state X-ray crystallographic study of **1**. In particular, both B3LYP [30] and BP86 [30b,31] functionals were used with the 6-311+G(d,p), 6-31+G(d), LanL2DZ, and SDD (vide infra) BS's for the organic framework, and two different BS's with relativistic effective core potentials for the metal ion [LanL2DZ [32], and Stuttgart RSC, [33] (SDD)]. Examination of the results of the above calculations (Table 3) allows one to deduce that: (a) the two BS's [6-311+G(d,p), 6-31+G(d)] used for the C, Cl, O and H yield very similar results, (b) the B3LYP functional with the same BS's (LanL2DZ) used for both the light atoms and the central metal ion, yields slightly overestimated bond distances and angles, compared to the solid-state experimental values; still, this level yields the best simulation for the Sn–O coordination bond than any other level tested, (c) the Stuttgard BS gives the poorest estimates, corresponding to the highest bond distances and angles, and (d) the BP86 functional with the same BS's used (LanL2DZ) for both the light atoms and the metal, yields larger values than the corresponding B3LYP functional calculation, for all coordination bond lengths, and this is also the case with the BP86/6-31+G(d) calculation.

Based on the above results obtained for **1**, DFT calculations with the B3LYP functional, using the same BS's (LanL2DZ) for both the light atoms and the central metal ion were performed on all complexes under examination.

2.8. Equilibrium geometries

All tables with the structural data for all complexes, their precursors, and the ligands PYR, PNO and DMP, under examination are given as Supplementary material. Selected geometrical parameters of the B3LYP/LanL2DZ optimized model compounds **1**–**4** and their precursors are given in Figs. 2–4. Since comparison between results in the gas and the solid state is not allowed, and owing to the lack of structural experimental studies in the gas phase for the same compounds, the gas-phase computed data is only compared in the figures.

Fig. 2 shows the computer plots and selected geometrical parameters of the B3LYP/LanL2DZ-optimized structures for the model compounds **1** and **3**. It is easily seen that in both cases, there is a pentacoordinate molecule of

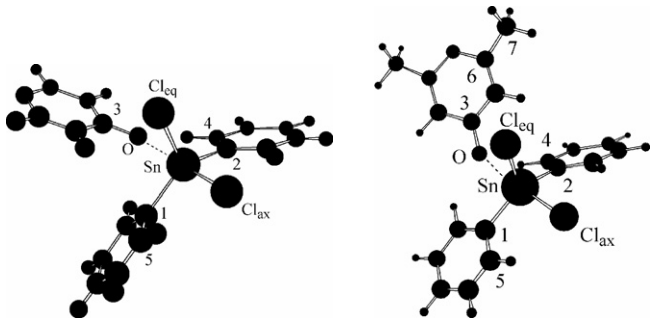

1 3

	Bond Lengths (Å)	
2.330	Sn–O	2.287
2.486	Sn–Cl_{ax}	2.495
2.457	Sn–Cl_{eq}	2.459
2.126	Sn–C(1)	2.129
2.132	Sn–C(2)	2.134
–	C(6)–C(7)	1.496
1.284	C(3)–O	1.289
	Bond Angles (°)	
173.2	Cl_{ax}–Sn–O	173.1
92.5	Cl_{ax}–Sn–Cl_{eq}	91.8
126.9	C(1)–Sn–C(2)	126.2
116.3	C(1)–Sn–Cl_{eq}	114.3
113.6	C(2)–Sn–Cl_{eq}	117.1
138.5	Sn–O–C(3)	138.7
	Dihedral Angles (°)	
68	Cl_{eq}–Sn–C(1)–C(5)	86.3
95.3	Cl_{eq}–Sn–C(2)–C(4)	112.1

Fig. 2. Computer plots and selected geometrical parameters of the B3LYP/LanL2DZ-optimized structures for the model compounds **1** and **3**.

Table 3
Selected optimized bond lengths (Å) and angles (°) calculated at the DFT level with different hybrid functionals and basis sets [BS's] on the model complex **1**

Functional	C,Cl,O,H BS	Sn BS	Sn–C[a]	Sn–C	Sn–Cl^{b}_{ax}	Sn–Cl^{c}_{eq}	Sn–O	C–Sn–C	Cl–Sn–Cl
B3LYP	LanL2DZ	LanL2DZ	2.132	2.126	2.486	2.457	2.330	126.9	92.5
	6-311+G(d,p)	LanL2DZ	2.137	2.131	2.425	2.381	2.478	126.1	95.9
	6-31+G(d)	LanL2DZ	2.138	2.134	2.427	2.389	2.474	125.8	94.2
	SDD	SDD	2.148	2.145	2.500	2.473	2.472	127.3	93.9
BP86	LanL2DZ	LanL2DZ	2.148	2.142	2.496	2.472	2.360	126.9	92.7
	6-31+G(d)	LanL2DZ	2.154	2.150	2.441	2.406	2.470	125.9	94.0

[a] Experimental values: Sn–C = 2.121, Sn–C = 2.133, Sn–Cl_{ax} = 2.431, Sn–Cl_{eq} = 2.365, Sn–O = 2.319 Å, C–Sn–C = 127.3°, Cl–Sn–Cl = 91.2°.
[b] Sn–Cl_{ax} stands for the Sn–Cl axial bond lengths.
[c] Sn–Cl_{eq} stands for the Sn–Cl equatorial bond lengths.

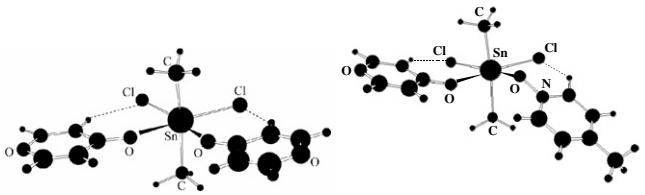

2 4

2		4
	Bond Lengths (Å)	
2.392	$Sn–O_{PYR}$	2.429
–	$Sn–O_{PNO}$	2.305
2.547	$Sn–Cl_{PYR}'$	2.548
–	$Sn–Cl_{PNO}'$	2.566
2.119	Sn–C	2.120
1.278	$C=O_{PYR}$	1.278
–	$N=O_{PNO}$	1.370
2.467	$H…Cl_{PYR}$	2.464
–	$H…Cl_{PNO}$	2.495
	Bond Angles (°)	
90.4	$Cl_{PYR}'–Sn–O$	90.9
–	$Cl_{PNO}'–Sn–O$	89.0
99.2	Cl–Sn–Cl	99.5
165.2	C–Sn–C	166.3
80.0	O–Sn–O	80.7

Fig. 3. Computer plots and selected geometrical parameters of the B3LYP/LanL2DZ-optimized structures for the model compounds **2** and **4**. (Primes denote *trans*-configuration, with respect to the corresponding group).

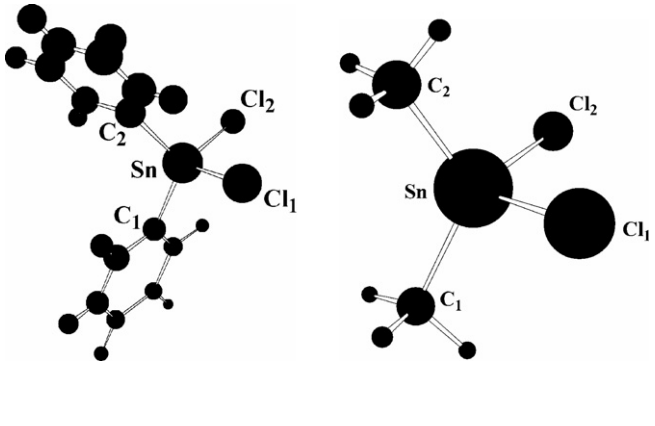

5 6

5		6
	Bond Lengths (Å)	
2.411	Sn–Cl	2.414
2.108	Sn–C	2.116
	Bond Angles (°)	
110.8	Cl(1)–Sn–C(1)	106.8
105.8	Cl(2)–Sn–C(1)	106.8
105.2	Cl(1)–Sn–Cl(2)	107.1
117.7	C(1)–Sn–C(2)	121.6

Fig. 4. Computer plots and selected geometrical parameters of the B3LYP/LanL2DZ-optimized structures for the precursor model compounds **5** and **6**.

trigonal-bipyramidal geometry, in close agreement with the X-ray crystal data of **1**. Two carbon atoms of the two different phenyl groups and one chlorine atom are located in the equatorial plane, the second Cl and the carbonyl O atom of the PYR ligand lie at the axial positions. The most significant change in the coordination sphere, between the two structures is the shortening (ca. 0.04 Å) of the Sn–O bond length, on passing from **1** to **3**. This is further substantiated by the corresponding Sn–O overlap population values, being 0.0274 and 0.0323 e for **1** and **3**, respectively, and the ν(Sn–O) vibrational frequency values (vide infra). Moreover, the two phenyl rings are mutually twisted with respect to the equatorial plane, to avoid steric congestion. The dihedral angles between the rings, defined by C(1)–C(5) and C(2)–C(4) and the trigonal plane, are 113.9° and 86.2°, and 95.6° and 69.8° for **1** and **3**, respectively, showing a stronger steric effect in the latter complex, in line with the closer proximity to Sn ion of the DMP and its different orientation opposite the two phenyl rings, compared to the PYR ligand. The sum of the equatorial angles in the trigonal girdle subtended at Sn by the two ipso carbons and the Cl are almost identical (357.7° and 357.6°, for **1** and **3**, respectively). The pyrone rings in **1** and **3**, are not positioned between the two phenyl groups, when viewing along the apical O–Sn–Cl axis, in close agreement with the analogous X-ray crystal data of **1**.

Fig. 3 exhibits the computer plots and selected geometrical parameters of the B3LYP/LanL2DZ-optimized structures for the model compounds **2** and **4**. It is easily seen that, contrary to the model complexes **1** and **3**, in the present case there is a hexacoordinated molecule of distorted compressed octahedral geometry. The two carbon atoms of two different methyl groups, lying *trans*- to each other, occupy the axial positions, and the two chlorine atoms (located *cis*- to each other), along with the two carbonyl O atoms of two different PYR and/or the PYR and PNO ligands, form the equatorial plane. All the four equatorial atoms lie on the same plane (dihedral angles of −0.3° and 3.5° for **2** and **4**, respectively). The most salient feature of these structures is the formation of two Cl···H linkages (=2.467 Å for the PYR ligands and 2.495 Å for the PNO one) between the equatorial Cl atoms and the H of the ortho- carbon atoms, strengthening further, the whole structures. As a consequence (i) the two PYR molecules lie on the same equatorial plane of **2** with the two Cl atoms and the Sn ion, however (ii) in **4**, the PYR and PNO ligand planes form 26.2° and −125.2° dihedral angles, respectively, with the equatorial plane, probably to avoid steric encumbrance. Hence, there is a stronger steric effect in **4**, in line with the closer proximity to Sn metal ion of the PNO ligand. The $Sn–O_{PYR}$ bond length is longer by ca. 0.04 Å in **4**, compared to that in **2**, all of the rest mutual structural parameters remain almost unchanged. It should be stressed out here that, upon the PYR and/or PNO ligands coordination, there is a medium Cl–Sn–Cl angle closing (by ca. 7–8°), followed by a concomitant significant C–Sn–C angle opening (by ca. 44°), compared to the

precursor Me_2SnCl_2 complex (vide infra). This is probably due to the approaching point of the two PYR and/or the PYR and PNO ligands, lying in-between the two Me groups of the Me_2SnCl_2 precursor. Hence, the steric effect of the two PYR and/or the PYR and PNO coordination would be stronger on the two Me groups, resulting to a significant C–Sn–C angle opening, and weaker on the Cl–Sn–Cl one. The $Sn–O_{PYR}$ bond length is longer than the corresponding lengths of the pentacoordinate complexes **1** and **3**, (by ca. 0.06–0.1 Å, respectively), while the $Sn–O_{PNO}$ is shorter than the $Sn–O_{PYR}$ one in **1**. This could be due to the weaker coordination of the PYR ligands and the stronger one of the PNO, in close agreement with both (i) the corresponding Sn–O overlap population values of 0.0239 e and 0.0257 e (0.0636 e for the $Sn–O_{PNO}$), and (ii) the ν(Sn–O) vibrational frequency values (vide infra). The sum of the equatorial angles in the tetragonal girdle subtended at Sn by the two PYR and/or the PYR and PNO carbonyl O atoms and the two Cl ones is 360°.

In Fig. 4 the computer plot and selected geometrical parameters of the B3LYP/LanL2DZ-optimized structures for the two model precursors **5** and **6** are given. Both complexes present a distorted tetrahedral geometry, as a result of different corresponding Sn–Cl and Sn–C bond lengths and angles. Two carbon atoms of two different methyl or phenyl groups, and two chlorine atoms occupy the four apices. It is interesting to note that despite the almost identical corresponding bond lengths, their corresponding bond angles are different. As a matter of fact, the Cl–Sn–Cl and C–Sn–C angles are larger in **6** by ca. 2° and 4°, respectively, compared to those of **5**, possibly due to the weaker steric effect of the two Me groups, to that of the phenyls.

2.9. Vibrational frequencies

Frequency values calculated at the B3LYP level contain known systematic errors that produce an overestimation compared to the experimental values. Therefore, it is usual to scale frequencies predicted at the B3LYP model of DFT theory by an empirical factor of 0.9610 [34]. The harmonic oscillator approach, which is used for calculated frequencies, usually produces higher values than the fundamental ones.

From all frequency values of the complexes only a few have been properly scaled and their values are given in Table 4. Those were chosen based upon the importance of the bond and the intensity of the corresponding absorption.

PYR and DMP ligands, for instance, are mostly characterized by the C=C and C=O stretching bands, while PNO by the N–O one. Table 4 includes the scaled calculated frequency values for the above bands, along with the vibrating atoms. The frequencies given in Table 4, are well characterized as stretch bands, since both their atom's orientation and eigenvector orientation lie on a single plane.

The first band examined corresponds to the pyrone C=O stretching frequency, appearing at 1657.2 and 1652.7 cm^{-1}, for PYR and DMP, respectively. These values are in very good agreement with the only existing vapor-phase C=O stretching frequency value of six 2-cyclohexane-1 ones, occurring in the region of 1710–1691 cm^{-1} [35]. For the two C=C scaled calculated stretching frequencies of the same ligands, as well as for the N–O one of the PNO there are not vapor-phase values to compare with. Nevertheless, both PYR and DMP ligands exhibit very similar corresponding C=O and C=C scaled calculated stretching frequencies.

Frequency information from infrared and Raman spectra in the gas-phase is not available for any of the complexes under study. Table 4 shows that contrary to **2**, exhibiting two ν(C=O) stretching bands, **1**, **3** and **4**, show only one, and this is also the case with the ν(Sn–O) stretching bands. As expected, the corresponding ν(C=O) stretching frequencies of all complexes are lowered, upon complexation, by ca. 145 cm^{-1}, compared to those of the

Table 4
Selected scaled, B3LYP/LanL2DZ-calculated, harmonic frequencies [cm^{-1}] of the model complexes **1**, **2**, **3** and **4**, and the PYR, DMP and PNO Ligands

Ligand/complex	ν(C=C)$_{sym}$	ν(C=C)$_{asym}$	ν(C=O)$^{a}_{sym}$	ν(C=O)$_{asym}$	$\Delta\nu$(C–O)[b]	ν(Sn–C)$_{sym}$	ν(Sn–C)$_{asym}$	ν(Sn–O)$_{sym}$	ν(Sn–O)$_{asym}$	ν(Sn–Cl)$_{eq}$	ν(Sn–Cl)$_{ax}$
PYR	1604.6	1540.9	1657.2								
DMP	1622.5	1580.6	1652.7								
PNO			1261.6								
1	1607.1	1520.7	1510.4		147	640.9[c]	646.5[c]	507.1		300.6	278.7
2	1610.4	1527.9	1618.2	1519.7	135	[d]	550.9	506.0	502.2	253.4[e]	248.5[f]
3	1632.3	1566.4	1507.7		145	641.1[c]	646.4[c]	509.5		298.1	274.2
4	1613.2	1527.8	1518.8		138	[d]	546.0[c]	500.6		251.8[e]	244.0[f]
			(1141.7)[g]		(120)			[d]			

[a] PYR and DMP ligands, and complexes **1** and **3** exhibit only one ν(C=O) vibrational frequency, and this is also the case with the ν(Sn–O) one of complexes **1** and **3**; PNO ligand exhibits only one ν(N–O) vibrational frequency, while complex **4** one ν(N–O) and one ν(C=O) vibrational frequencies.
[b] $\Delta\nu(C–O) = [\nu(C–O)_{lig} - \nu(C–O)_{compl}]$.
[c] Frequency vibrations exhibiting low IR intensities.
[d] Not determined.
[e] ν(Sn–Cl) asymmetric vibration.
[f] ν(Sn–Cl) symmetric vibration.
[g] Numbers in parentheses correspond to the PNO ligand vibrational frequency values of **4**.

ligands; the same holds also true for the ν(N–O) stretching frequency of **4**, the corresponding lowering upon complexation amounting to ca. 120 cm^{-1}. Moreover, for the same reason, the ν(C=C) stretching bands of the complexes, are lowered by ca. 13–20 cm^{-1} [$\nu(C{=}C)_{asym}$] or increased by ca. 2.5–10 cm^{-1} [$\nu(C{=}C)_{sym}$]. The ν(Sn–O) stretching-bands trend (**4** < **2** < **1** < **3**) is in excellent agreement with that (**2** > **1** > **3** > **4**) expected on the basis of the corresponding Sn–O bond lengths. Finally, it is well known [35] that formation of a hydrogen bond, leads to a stretching frequency shift towards a lower value the neighbouring bonds. This is also, in excellent agreement with the lowering (by ca. 35–49 cm^{-1}) of both ν(Sn–Cl) stretching bands in **2** and **4**, (in which two H···Cl bonds are formed) compared to those in **1** and **3**.

2.10. Reactivity of the complexes

Prompted by the above experimental reactivity findings, we initiated a systematic quantum-chemical investigation in an attempt to understand the reactivity of both the PYR and DMP ligands towards the Sn ions. In particular, B3LYP/6-311+G(d,p) calculations, with a natural bond analysis, were carried out on both ligands, which were combined with the calculations described above for the precursor complexes **5** and **6**.

The most salient features of the ground-state electronic structure of PYR and DMP, are their HOMO's, which are schematically depicted in Fig. 5. In particular, the two HOMO's are almost identical, mostly centered on the carbonyl O atom. The nature of the two HOMO's, along with the high frontier density values, P_r(HOMO) [36] for the carbonyl O atom, (0.37 and 0.37, respectively) and their high, calculated, negative charges, ($q_r = -0.58$ e and -0.60 e, respectively), strongly suggest that (i) the latter atom should be the nucleophilic center for Sn(IV) attack of either ligand, and (ii) both ligands show identical nucleophilic ability.

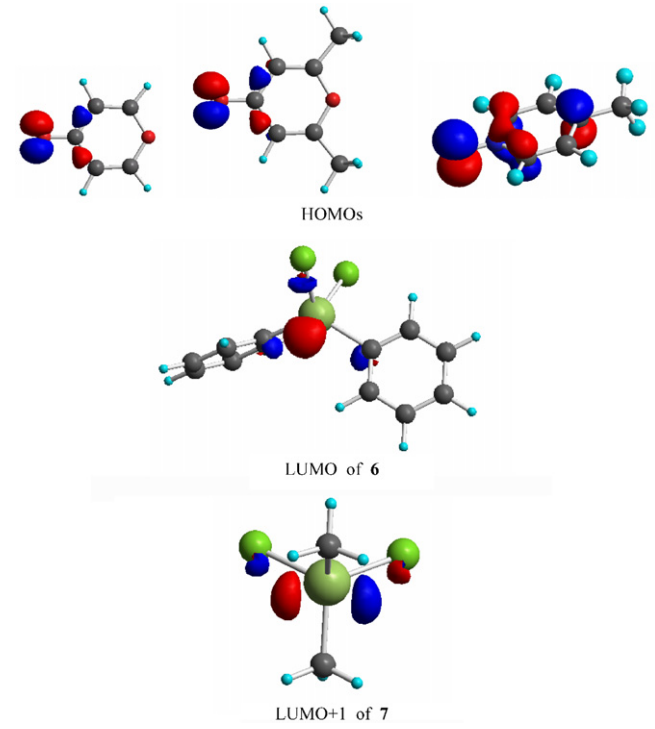

Fig. 5. The LUMO and LUMO + 1 of the precursor model compounds **5** and **6**, respectively, and the HOMO's of the PYR, DMP and PNO ligands.

Fig. 5 also presents the LUMO and LUMO + 1 of the two precursor complexes **5** and **6**, respectively. It is easily seen that in both cases, the LUMO's are located mainly on the central Sn ion. In particular, in the LUMO of **5** there is only one vacant lobe directed *trans*- to one of the Cl atoms. Hence, the LUMO–HOMO interaction between the **6** and the PYR ligand should yield complex **1**, in excellent agreement with the X-ray experimental structural data of the latter complex. However, in the case of **6**, possibly due to the weaker than in **5** steric repulsions, two vacant lobes appear in its LUMO + 1, directed *trans*- to its two Cl atoms. Hence, a (LUMO + 1)–HOMO interaction, like above, should yield complex **2**, in excellent agreement with the theoretical structural data of the latter complex. Moreover, due to the positive charge on the Sn(IV) ion (ca. 1.00 e), in both **5** and **6**, the nucleophilic attack described above, should be both a charge- and frontier-orbital-controlled one.

Finally, the possible mechanism of formation of the **4** adduct (the monoexchange from **2**), was also investigated with the aid of additional calculations, described below.

The nature of the FMO's of the PNO ligand and its nucleophilic ability was investigated first. The π-type HOMO of PNO, mostly centered on the O atom of the N–O group, is also shown in Fig. 5. Moreover, its HOMO − 1 is quite analogous to the HOMO's of PYR and DMP. The nature of the two FMO's of PNO, along with the rather lower than the PYR frontier density value, P_r(HOMO) of its carbonyl O atom, (0.28 compared to 0.37), and its, almost equal to the PYR, calculated negative charge, ($q_r = -0.55$ e compared to -0.58 e), could suggest that (a) its carbonyl O atom should also be the nucleophilic center for Sn(IV) attack, and (b) PNO shows an inferior than the PYR nucleophilic ability.

Next, an additional B3LYP/LanL2DZ calculation was performed, in the search of a sevencoordinate transition state (TS), involving the adduct **2** and a PNO ligand, lying at the equatorial plane of **2**, in between its two PYR ligands, namely:

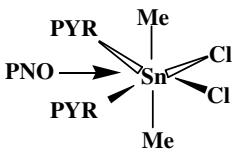

The latter TS, if any, should correspond to a S_N^2 mechanistic scheme for the formation of the **4** adduct. However, calculations failed to afford a TS stationary point of that kind. This is in close agreement with the inferior nucleophilic

ability of the PNO ligand compared to that of PYR. Hence, a S_N2 mechanism could be excluded for the corresponding mechanism of formation. Moreover, additional calculations have shown that the dissociation of **2** to the monosubstituted Sn complex and the PYR ligand (Eq. (4) below) requires an energy of only 9.7 kcal/mol, showing that this dissociation could easily occur at room temperature in solution. This is in close agreement with the large dissociation observed experimentally in solution for the adduct **2**, (vide supra). Hence, a S_N1 formation mechanism rather than a S_N2 one seems most probable for **4**, namely:

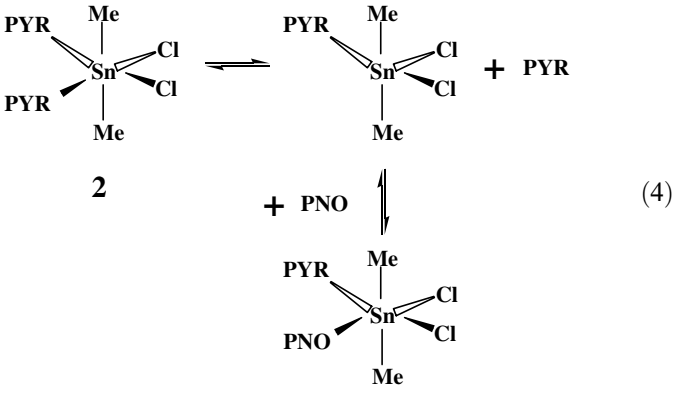

(4)

3. Conclusion

The adducts Ph_2SnCl_2(PYR) (**1**), $Me_2SnCl_2(PYR)_2$ (**2**), Ph_2SnCl_2(DMP) (**3**) and Me_2SnCl_2(PYR)(PNO) (**4**), have been prepared by the addition of the corresponding γ-pyrone (PYR or DMP) to chloroform solution of R_2SnCl_2, and characterized analytically and spectroscopically. Moreover, the single-crystal X-ray diffraction study of **1** shows the Sn(IV) to be five-coordinated, and the PYR ligand is attached to the metal via its carbonyl O. The reactivity of **2** towards bipy, Ph_3PO, QNO (Q = quinoline) resulted in complete displacement of PYR, whereas, the PNO displaced only one equivalent of PYR, causing the preparation of the new mixed complex **4,** possibly via a S_N1 formation mechanism. DFT/B3LYP molecular orbital calculations carried out for the **1**–**4** complexes, their precursors, Ph_2SnCl_2, (**5**) and Me_2SnCl_2, (**6**) and the ligands, PYR and DMP explained the structures, vibrational frequencies, and the electron-accepting ability of the complexes, and the reactivity of their precursors towards nucleophiles.

4. Experimental

4.1. General procedures

All the reactions were performed in air at room temperature. Me_2SnCl_2, was purchased from Alfa Products Ventron, whereas Ph_2SnCl_2, DMP and PYR from Aldrich. C, H and N analyses were carried out in our microanalytical laboratory with a Perkin Elmer 240 instrument. Melting points were determined in open tubes. IR spectra were recorded on a Perkin Elmer FT 16500 spectrometer and samples prepared as KBr disks. The far-IR spectra were taken on Bruker FT IR IFS 113v spectrometer (resolution 2 cm^{-1}, 64 scans) as polyethylene disks. ^1H and ^{13}C NMR spectra were measured on a Brucker 300 spectrometer. ^{119}Sn Mössbauer spectra of powder samples were obtained at 85 K in an exchange gas cryostat, using a constant acceleration spectrometer and a 10 mCi calcium stannate source kept at room temperature. Spectrometer calibration was effected using a metallic iron foil. Isomer shifts were reported relative to $CaSnO_3$, assuming that they are the same as those of the $BaSnO_3$. The chloroform solutions of all the new adducts do not show appreciable electrical conductivity.

4.2. Synthesis of Ph_2SnCl_2(PYR) (1)

PYR (0.048 g, 0.5 mmol) was added to a solution of Ph_2SnCl_2 (0.172 g, 0.5 mmol) in $CHCl_3$ (15 mL), under constant stirring. The reaction mixture was stirred for 1 h and left to concentrate slowly in air, affording crystals of the product. The off white crystals were collected by suctional filtration and were recrystallized from $CHCl_3$, dried in vacuo. X-ray quality crystals of **1** were grown from $CHCl_3$. Yield (0.079 g, 36%).

Mp 100–101 °C. ^1H NMR (300 MHz, $CDCl_3$): $\delta = 7.8$ (d, ^3J H_b, $H_a = 5.4$ Hz, 2H, 2,6 of PYR), 6.4 (d, ^3J H_a, $H_b = 5.4$ Hz, 2H, 3,5 of PYR), 7.9–7.7 (m, 10H, Sn–Ph_2) ppm. ^{13}C NMR (75 MHz, $CDCl_3$): $\delta = 155.4$ (2C, 2,6 PYR), 118.4 (2C, 3,5 of PYR), 178.5 (1C, C=O), $\delta =$ 139.7 (^1J C, $^{119}Sn = 891.1$ Hz, 2C, ipso Sn–Ph_2, ^1J C, $^{117}Sn = 849.6$ Hz, 2 C, ipso Sn–Ph_2), 135.2 (^2J C, $^{119}Sn =$ 69.5 Hz, 2C, *ortho* Sn–Ph_2), 129.2 (^3J C, $^{119}Sn = 90.3$ Hz, 2C, *meta* Sn–Ph_2) 131.02 (^4J C, $^{119}Sn = 17.1$ Hz, 2C, *para* Sn–Ph_2) ppm. IR (KBr pellets, cm^{-1}): $\nu = 1688$ (vw), 1673 (vw), 1639 (vs, broad), 1566 (sh), 1560 (vs), 1533 (sh), 1479 (w), 1446 (w), 1430 (m), 1394 (vw), 1324 (s), 1225 (vw), 1198 (m), 997 (w), 937 (sh), 930 (s), 863 (w), 856 (m), 850 (w), 846 (w), 835 (w, broad), 695 (vs, broad), 669 (vw), 526 (m), 520 (m), 481 (m), 476 (m), 469 (s, broad), 458 (s, broad) 444 (m), 340 (w), 292 (m), 277 (m), 285 (m) cm^{-1}. Anal. Calc. for $C_{17}H_{14}O_2Cl_2Sn$ (439.91): C, 46.42; H, 3.34. Found: C, 46.28; H, 3.34%.

4.3. Synthesis of $Me_2SnCl_2(PYR)_2$ (2)

PYR (0.096 g, 1 mmol) was added to a solution of Me_2SnCl_2 (0.109 g, 0.5 mmol) in $CHCl_3$ (10 mL). The solution was stirred for 1 h and became slightly turbit. Then, it was filtrated and to the clear pale yellow filtrate petroleum ether (bp 40–60 °C) was added (5 mL) and left aside to crystallize slowly. The mother liquid was discarded and the precipitated crystals were dried in air. The product was dissolved in a mixture of CH_2Cl_2 and petroleum ether and was left in the freezer affording big pale yellow crystals, which were dried in vacuo. Yield (0.105 g, 51%).

Mp 82–84 °C. ^{1}H NMR (300 MHz, $CDCl_3$): $\delta = 7.9$ (d, ^3J H_b, $H_a = 6.6$ Hz, 2H, 2,6 of PYR), 6.5 (d, ^3J H_a, $H_b = 6.6$ Hz, 2H, 3,5 of PYR), and 1.3 (s, ^2J ^{119}Sn, H = 79.4 Hz, ^2J ^{117}Sn, H = 76.3 Hz, 6H, $SnMe_2$) ppm. ^{13}C NMR (75 MHz, $CDCl_3$): $\delta = 178.5$ (1C, C=O), 156.3 (2C, 2,6 of PYR), 118.1 (2C, 3,5 of PYR), and 10.3 (^1J C, ^{119}Sn = 595.7 Hz, ^1J C, ^{117}Sn = 571.3 Hz, $SnMe_2$) ppm. IR (KBr pellets, cm^{-1}): $\nu = 1675$ (m), 1639 (s), 1579 (s), 1536 (m), 1435 (m), 1321 (s), 1376 (w), 1321 (s), 1229 (w), 1199 (m), 1036 (w), 1016 (w), 926 (s), 857 (s), 799 (w), 540 (w), 516 (w), 470 (w, broad), 461 (w, broad), 267 (w, broad), 261 (w, broad). Anal. Calc. for $C_{12}H_{14}O_4Cl_2Sn$ (411.86): C, 34.99; H, 3.43. Found: C, 34.97; H, 3.75%.

4.4. Synthesis of $Ph_2SnCl_2(DMP)$ (3)

The DMP (0.050g, 0.4 mmol) was added to a solution of Ph_2SnCl_2 (0.136 g, 0,4 mmol) in $CHCl_3$ (10 mL) contained in a small flask. The DMP was added under constant stirring which was kept for 3 h. Then petroleum ether (bp 40–60 °C) was added (~2 mL) and left aside to crystallize slowly in air affording big white crystals, which were dried in vacuo. Yield (0.120 g, 64%).

Mp 145–146 °C. ^{1}H NMR (300 MHz, $CDCl_3$): $\delta = 6.2$ (s, 2H, 3,5 of DMP), 2.3 (s, 6H, Me of DMP), and 7.9–7.5 (m, 10H, Sn–Ph_2) ppm. ^{13}C NMR (75 MHz, $CDCl_3$): $\delta = 167.2$ (2C, 2,6 DMP), 113.7 (2C, 3,5 of DMP), 180.9 (1C, C=O), 140.27 (^1J C, ^{119}Sn = 925.9 Hz, ^1J C, ^{117}Sn = 882.1 Hz, 2C, ipso Sn–Ph_2), 135.3 (^2J C, ^{119}Sn = 64.2 Hz, ^2J C, ^{117}Sn = 61.0 Hz, 2C, *ortho* Sn–Ph_2), 129.2 (^3J C, ^{119}Sn = 92.6 Hz, ^3J C, ^{117}Sn = 88.4 Hz, 2C, *meta* Sn–Ph_2) and 130.9 (^4J C, ^{119}Sn = 17.8 Hz, 2C, *para* Sn–Ph_2) ppm. IR (KBr pellets, cm^{-1}): $\nu = 1651$ (vs), 1599 (sh), 1576 (m), 1539 (vs), 1478 (m), 1447 (w), 1428 (m), 1417 (w), 1337 (m), 1199 (s), 1171 (w), 1063 (w), 1039 (w), 998 (w), 954 (w), 906 (m), 877 (m), 847 (w), 748 (m), 734 (s), 695 (s), 621 (m), 543 (m), 524 (w), 454 (m), 445 (w), 369 (vw), 333 (m), 270 (m) 243 (m), 202 (w). Anal. Calc. for $C_{19}H_{18}O_2Cl_2Sn$ (467.97): C, 48.45; H, 3.81. Found: C, 48.77; H, 3.88%.

4.5. Reactivity of $Me_2SnCl_2(PYR)_2$ (2)

(I) Addition of QNO (0.27 mmol) or bipy (0.2 mmol) to equimolar chloroform solutions of **2**, led to the complete displacement of PYR. After stirring for 1 h and addition of petroleum ether, the mixtures were left in air to concentrate slowly affording crystals of the known adducts $Me_2SnCl_2(QNO)_2$ [8] or Me_2SnCl_2(bipy) [18]. The reaction of QNO and the starting adduct **2** in 2:1 molar ratio and work up as above gave again the same product. (II) Addition of solid $OPPh_3$ (0.4 mmol) to a chloroform (0.2 mmol) solution of **2**, resulted in complete displacement of the PYR from the starting adduct. Work up as above gave the known solid $Me_2SnCl_2(OPPh_3)_2$ [18]. (III) The ligand PNO (0.092 g, 0.2 mmol) was added to a chloroform solution (10 mL) of **2** (0.082 g, 0.2 mmol), contained in a small beaker. The mixture was stirred for 1 h, then petroleum ether (2 mL) was added and left to crystallize slowly in air, affording off yellow crystals of the new product Me_2SnCl_2(PYR)(PNO) (**4**). Yield (0.059 g, 70%).

Mp 165–167 °C. ^{1}H NMR (300 MHz, $CDCl_3$): $\delta = 7.8$ (d, ^3J H_b, $H_a = 5.7$ Hz, 2H, 2,6 of PYR), 6.4 (d, ^3J, H_a, $H_b = 5.7$ Hz, 2H, 3,5 of PYR), 1.1 (s, ^2J H, ^{119}Sn = 87.2 Hz, ^2J H, ^{117}Sn = 83.4 Hz, 6H, $SnMe_2$), 7.4 (br, 2H, MeC_5H_4NO), 8.3 (br, 2H, MeC_5H_4NO) and 2.5 (s, 3H, MeC_5H_4NO) ppm. ^{13}C NMR (75 MHz, $CDCl_3$, 25 °C): $\delta = 155.5$ (2C, 2,6 PYR), 118.1 (2C, 3,5 of PYR), 177.9 (1C, C=O), 20.8 (s, 1C, MeC_5H_4NO) and 11.4 (^1J C, ^{119}Sn = 693.9 Hz, 2C, $SnMe_2$) ppm. IR (KBr pellets, cm^{-1}): $\nu = 1637$ (s), 1624 (w), 1560 (w), 1498 (s), 1482 (s), 1459 (s, broad), 1322 (w), 1243 (vw), 1201 (vs), 1184 (s), 1171 (s), 1121 (vw), 1108 (w), 1040 (w), 975 (vw), 956 (w), 930 (w), 854 (s), 842 (sh), 837 (s), 698 (vs), 669 (w), 662 (m), 567 (s), 530 (m), 482 (vs), 464 (vs), 390 (s), 321 (vw), 262 (vw), 231 (w), 151 (m). Anal. Calc. for $C_{13}H_{17}O_3Cl_2NSn$ (424.89): C, 36.75; H, 4.03; N, 3.29. Found: C, 36.82; H, 4.05; N, 3.46%.

4.6. X-ray crystal structure determination for 1

The crystal was mounted on a glass fibre and data were collected at 173 K on a Brucker SMART CCD area detector 3-circle diffractometer (Mo Kα X-radiation, graphite monochromator ($\lambda = 0.71073$ Å)). It was confirmed that crystal decay had not taken place during the course of the data collection. Narrow "frames" were collected for 0.3° increments in W for three settings of Φ. In each of these three cases a total of 1271 frames of data were collected affording rather more than a hemisphere of data. The substantial redundancy in data allows empirical absorption corrections (SADABS) [37] to be applied using multiple measurements of equivalent reflections. The data frames were integrated using SAINT [38]. The structure was solved by conventional direct methods and refined by full matrix least squares on all F^2 data using SHELXTL ver. 5.03 [39]. All non hydrogen atoms were refined with anisotropic thermal parameters. All hydrogen atoms were included in calculated positions with isotropic thermal parameter ca. 1.2 × (aromatic CH) the equivalent isotropic thermal parameters of their parent carbon atoms. Details of the crystal data and intensity collection are summarized in Table 5. All calculations were carried out on Silicon Graphics Iris Indigo or Indy computers.

4.7. Quantum-chemical calculations

For the reasons explained in another section of this study, the geometries of all minimum energy structures for all complexes and their corresponding precursors were fully optimized at the B3LYP/LanL2DZ level of theory; the PYR, DMP and PNO ligands at the B3LYP/6-311+G(d,p) level. C_1 point group symmetry for each species was assumed as the initial geometry of the optimization procedure. All calculations investigating the

Table 5
Crystal data and structure refinement for **1**

Formula	$C_{17}H_{14}Cl_{12}O_2Sn$
Fw	439.87
T (K)	173(2)
Crystal system	Monoclinic
Space group	$P2_1/c$
λ (Å)	0.71073
a (Å)	8.452(2)
b (Å)	9.3752(13)
c (Å)	21.405(4)
β (°)	92.76(2)
V (Å^3)	1694.1(6)
Z	4
D_{calc} (g/cm^3)	1.725
μ (mm^{-1})	1.826
$F(000)$	864
Crystal size (mm)	0.50 × 0.20 × 0.15
θ Range for data collection (°)	1.90–27.50
Index ranges	$-10 \leqslant h \leqslant 10$, $-12 \leqslant k \leqslant 12$, $-27 \leqslant l \leqslant 27$
Reflections collected	16,895
Independent reflections (R_{int})	3865 (0.0243)
Absorption correction	SADABS
Maximum and minimum transmission	0.646824 and 0.509887
Refinement method	Full-matrix least-squares on F^2
Data/restraints/parameters	3865/0/199
Goodness-of-fit on F^2	1.057
R_1, wR_2, ($I > 2\sigma(I)$)	0.0193, 0.0459
R_1, wR_2 (all data)	0.0232, 0.0469
Weighting scheme	Calc $w = 1/[s^2(F_o^2) + (0.0244P)^2 + 0.0000P]$ where $P = (F_o^2 + 2F_c^2)/3$
Largest difference in peak/hole (e Å^{-3})	0.255/−0.615

structural parameters of the molecules addressed here are based on final frequency calculations that provide energy minima with certainty. For each molecule full optimization calculations were performed in an attempt to determine the closest structure to the global minimum. The non-appearance of negative frequencies was assumed to be evidence for a global potential energy minimum of each calculated structure. Although the use of all-electron basis sets provides better accuracy, pseudopotential techniques are useful when relativistic effects have to be taken into account. Thus, the LanL2DZ BS's with relativistic effective core potentials were tested for all complexes of‘ this study. The GAUSSIAN-03W software package [40] was used.

Appendix A. Supplementary material

CCDC 657306 contains the supplementary crystallographic data for **1**. These data can be obtained free of charge from The Cambridge Crystallographic Data Centre via www.ccdc.cam.ac.uk/data_request/cif. Cartesian coordinates for the B3LYP/LanL2DZ optimized **1**, **2**, **3**, **4**, **5** and **6** and the B3LYP/6-311+G(d,p) optimized PYR, DMP and PNO structures. Supplementary data associated with this article can be found, in the online version, at doi:10.1016/j.jorganchem.2008.01.014.

References

[1] E.M. Brigs, A.E. Hill, J. Chem. Soc. A (1969) 1835 and references therein.
[2] S. Sitran, D. Fregona, G. Faraglia, J. Coord. Chem. 20 (1989) 193, and references therein.
[3] G. Faraglia, Z. Guo, S. Sitran, Polyhedron 10 (1991) 351.
[4] D. Fregona, G. Faraglia, S. Sitran, J. Coord. Chem. 30 (1993) 221.
[5] D. Fregona, Z.J. Guo, G. Faraglia, S. Sitran, J. Coord. Chem. 28 (1993) 73.
[6] H. Papadaki, A. Christofides, J.C. Jeffery, T. Bakas, J. Coord. Chem. 47 (1999) 559.
[7] I. Saura-Liamas, D.M. Dalton, A.M. Artif, J.A. Gladysz, Organometallics 11 (1992) 683.
[8] D. Fregona, Z.J. Guo, G. Faraglia, S. Sitran, Transition Met. Chem. 17 (1992) 242.
[9] Q. Lin, W.K. Leong, Organometallics 22 (2003) 3639.
[10] M. Gielen, Appl. Organomet. Chem. 16 (2002) 481.
[11] V. Valla, M. Bakola-Christianopoulou, Synth. React. Inorg. Met.-Org. Nano-Met. Chem. 37 (2007) 507.
[12] G. Wilkinson, F.G.A. Stone, E.W. Abel, Comprehensive Organometallic Chemistry, vol. 2, Pergamon Press, Oxford, 1982, p. 616 (chapter II) and references therein.
[13] A.L. Rheingold, S.W. Ng, J.J. Zuckerman, Organometallics 3 (1984) 233.
[14] S.W. Ng, V.G. Kumar Das, Z. Kristallogr. 209 (1993) 744.
[15] E.A. Blom, B.R. Penfold, N.T. Robinson, J. Chem. Soc. A (1969) 913.
[16] S.W. Ng, J.J. Zuckerman, J. Chem. Soc., Chem. Commun. (1982) 475.
[17] D. Cunningham, J. Douek, M.J. Fraser, M. Mc Partlin, J. Organomet. Chem. C23 (1975) 90.
[18] J.P. Clark, C.I. Wilkins, J. Chem. Soc. A (1966) 871.
[19] A.R. Katritzky, R.A. Jones, Spectrochim. Acta 17 (1961) 64.
[20] J.H. Looker, W.W. Hanneman, J. Org. Chem. 27 (1962) 381.
[21] M.M. Finnegan, T.G. Lutz, W.O. Nelson, A. Smith, C. Orvig, Inorg. Chem. 26 (1987) 2171.
[22] W.F. Howard Jr., R.W. Crecely, W.H. Nelson, Inorg. Chem. 24 (1985) 2204.
[23] W. Kitching, V.G. Kumar Das, Aust. J. Chem. 21 (1968) 2401.
[24] T.A.K. Al-allaf, J. Organomet. Chem. 306 (1986) 337.
[25] V.G. Kumar Das, Y. Chee-Keong, P.J. Smith, J. Organomet. Chem. 327 (1987) 311.
[26] B.W. Fitzsimmons, N.J. Sealey, A.W. Smith, J. Chem. Soc. A (1969) 143.
[27] T.N. Srivastava, P.C. Srivastava, J.S. Gaur, Indian J. Chem. A 17 (1979) 142.
[28] R.W.J. Wedd, J.R. Sams, Can. J. Chem. 48 (1970) 71.
[29] (a) E.S. Kryachko, E.V. Ludena, Energy Density Functional Theory of Many Electron Systems, Kluwer Academic Publisher, Dordrecht, 1990;
(b) W. Koch, M.C. Holthausen, A Chemist's Guide to Density Functional Theory, 2nd ed., Wiley-VCH, Stuttgart, 2002.
[30] (a) A.D. Becke, J. Chem. Phys. 98 (1993) 5648;
(b) A.D. Becke, Phys. Rev. A 38 (1988) 3098;
(c) C. Lee, W. Wang, R.G. Parr, Phys. Rev. B 37 (1988) 785.
[31] J.P. Perdew, Phys. Rev. B 33 (1986) 8822.
[32] J.V. Ortiz, P.J. Hay, R.L. Martin, J. Am. Chem. Soc. 114 (1992) 2736.
[33] (a) P. Fuentealba, H. Preuss, H. Stoll, L.V. Szentpaly, Chem. Phys. Lett. 89 (1982) 418;
(b) A. Bergner, M. Dolg, W. Kuechle, H. Stoll, H. Preuss, Mol. Phys. 80 (1993) 1431;
(c) P. Fuentealba, L.V. Szentpaly, H. Preuss, H. Stoll, J. Phys. B 18 (1985) 1287;

(d) G. Igel-Mann, H. Stoll, H. Preuss, Mol. Phys. 65 (1988) 1321;
(e) M. Dolg, U. Wedig, H. Stoll, H. Preuss, J. Chem. Phys. 86 (1987) 866;
(f) M. Dolg, H. Stoll, H. Preuss, R.M. Pitzer, J. Phys. Chem. 97 (1993) 5852.

[34] A.P. Scott, L. Radom, J. Phys. Chem. 100 (1996) 16502.

[35] D. Lin-Vien, N.B. Coltharp, W.G. Fateley, J.G. Grasselli, The Handbook of Infrared and Raman Characteristic Frequencies of Organic Molecules, Academic Press, San Diego, 1991.

[36] K. Fukui, H. Fujimoto, Tetrahedron Lett. (1965) 4303.

[37] G.M. Sheldrick, SADABS, A Program for Absorption Correction with the Siemens SMART System, University of Göttingen, 1996.

[38] SAINT Integration Software, Siemens Analytical X-ray Instruments Inc., Madison, WI, 1994.

[39] SHELXTL 5.03 Program System, Siemens Analytical X-ray Instruments, Madison, WI, 1995.

[40] M.J. Frisch, G.W. Trucks, H.B. Schlegel, G.E. Scuseria, M.A. Robb, J.R. Cheeseman, J.A. Montgomery Jr, T. Vreven, K.N. Kudin, J.C. Burant, J.M. Millam, S.S. Iyengar, J. Tomasi, V. Barone, B. Mennucci, M. Cossi, G. Scalmani, N. Rega, G.A. Petersson, H. Nakatsuji, M. Hada, M. Ehara, K. Toyota, R. Fukuda, J. Hasegawa, M. Ishida, T. Nakajima, Y. Honda, O. Kitao, H. Nakai, M. Klene, X. Li, J.E. Knox, H.P. Hratchian, J.B. Cross, C. Adamo, J. Jaramillo, R. Gomperts, R.E. Stratmann, O. Yazyev, A.J. Austin, R. Cammi, C. Pomelli, J.W. Ochterski, P.Y. Ayala, K. Morokuma, G.A. Voth, P. Salvador, J.J. Dannenberg, V.G. Zakrzewski, S. Dapprich, A.D. Daniels, M.C. Strain, O. Farkas, D.K. Malick, A.D. Rabuck, K. Raghavachari, J.B. Foresman, J.V. Ortiz, Q. Cui, A.G. Baboul, S. Clifford, J. Cioslowski, B.B. Stefanov, G. Liu, A. Liashenko, P. Piskorz, I. Komaromi, R.L. Martin, D.J. Fox, T. Keith, M.A. Al-Laham, C.Y. Peng, A. Nanayakkara, M. Challacombe, P.M.W. Gill, B. Johnson, W. Chen, M.W. Wong, C. Gonzalez, J.A. Pople, GAUSSIAN 03, Revision B.03, Gaussian, Inc., Pittsburgh, PA, 2003.